Journal of Catalysis 257 (2008) 215–220

Contents lists available at ScienceDirect

Journal of Catalysis

www.elsevier.com/locate/jcat

Synthesis, characterization and catalytic activities of μ–oxo-bridged binuclear iron complexes encapsulated in SBA-15

Haijun Chen [a], Satoru Kuranari [a], Tsukasa Akiyama [a], Jinlong Zhang [b], Masakazu Anpo [a,*]

[a] Department of Applied Chemistry, Graduate School of Engineering, Osaka Prefecture University, 1-1 Gakuen-cho, Naka-Ku, Sakai, Osaka 599-8531, Japan
[b] Institute of Fine Chemicals, East China University of Science and Technology, 130 Meilong Road, Shanghai 200237, PR China

ARTICLE INFO

Article history:
Received 11 March 2008
Revised 3 May 2008
Accepted 6 May 2008
Available online 29 May 2008

Keywords:
Binuclear Fe^{3+} complex
Cyclohexane oxidation
SBA-15

ABSTRACT

Fe^{3+} bipyridine complexes were successfully anchored on the inner surface of the mesopores of SBA-15 and compared with those immobilized on the surface of SiO_2. FT-IR, ESR, and XAFS measurements were used to characterize the structure of the formed μ–oxo-bridged binuclear Fe bipyridine complexes inside the mesopores of SBA-15, which were observed to be the active species for the oxidation of cyclohexane. Furthermore, binuclear Fe complexes anchored inside the mesopores of SBA-15 were found to show much higher activity than those anchored on the surface of SiO_2. The effect of the presence of the Si–OH groups on the surface of SiO_2 on the selectivity for the oxidation of cyclohexane into cyclohexanone also was investigated.

1. Introduction

The development of catalytic systems for the oxidation of hydrocarbon is of great importance for the direct conversion of methane to methanol, which can be considered an efficient route for the production of liquid fuel [1–3]. Some bacteria are capable of conducting this reaction through enzyme methane monooxygenase (MMO) [4]. The μ–oxo diferric complexes representing structural mimics of the active center of these enzymes [5,6] have received much attention, and their unique structures have prompted the design of new bio-inspired di-iron catalysts for hydroxylation, epoxidation, and sulfoxidation reactions. Among them, di-iron complexes with polypyridine/nitrogen ligands have been applied to enantioselective catalysis for epoxidation [7–10].

For homogeneous catalytic reactions, the origin of the activity of the metal complexes is generally considered the elimination of one or more of the bonding ligands from its central metal. Thus, the formed vacant site of the metal plays an important role in the access of the reactants to the metal. As a result, metals with vacant sites or unsaturated coordination sites exhibit catalytic activity, whereas the saturation of such vacant sites for the metal results in a decrease in reactivity and loss of catalytic activity for the metal complexes [11,12]. In recent years, the immobilization of transition metal complexes on the surface of the supports or the encapsulation of the transition metal complexes inside the porous materials has received considerable attention. Such applications can result in a significant enhancement of novel catalytic activities that homogeneous complexes do not exhibit [13–15]. Cyclometalated platinum(II) complexes anchored into the pore channels of ordered mesoporous silica SBA-15 have been reported to lead to a 100-fold increase in the efficiency of the photosensitized oxidation compared with the reactivity of the cyclometalated platinum(II) complexes present in Nafion membrane supports [15]. Moreover, the covalent immobilization of CuBr/SdMBpyTMS complexes into porous silica [CPG(240)] allows polymerizations of methyl methacrylate to achieve reasonably high conversion with narrow molecular weight distributions [16]. In addition, a protection effect of the matrix over the active centers has been evidenced for the μ–oxo-bridged dinuclear iron 1,10-phenanthroline (Fe-phen) complexes impregnated in MCM-41. The Fe–O–Fe bridges of the Fe-SBA catalyst cleave to form an isolated single Fe species during the oxidation of benzyl alcohol, whereas this remains stable in an encapsulated system [17].

Methods for incorporating metal complexes into substrates includes physical adsorption [18], ion exchange [19], encapsulation [20], and other techniques [21–26], whereas the incorporation of metal complexes using methods other than the formation of covalent linkages likely will result in significant leaching of the complexes from the solid substrates during the reactions [27]. Datye et al [28,29] functionalized the surface of mesoporous silicas with 3-aminopropyltrimethoxysilane, which can help prevent the thermal sintering of gold nanoparticles. In this study, 4,4′-dimethyl-2,2′-bipyridyl (dMBpy) was modified to react with 3-aminopropyltriethoxysilane, so that bipyridine ligands could be tethered to the inner surface of the mesoporous silica SBA-15 [30,31]. These ligands were heterogeneously metalated with $Fe(ClO_4)_3$ to obtain anchored binuclear iron complexes. The reactivity of these

* Corresponding author. Fax: +81 72 254 9910.
E-mail address: anpo@chem.osakafu-u.ac.jp (M. Anpo).

0021-9517/$ – see front matter
doi:10.1016/j.jcat.2008.05.003

binuclear iron complexes anchored inside the mesopores of SBA-15 for the oxidation of cyclohexane was then investigated.

2. Experimental

2.1. Preparation of SBA-CH_3

SBA-15 was synthesized using the triblock poly(ethylene oxide)–poly(propylene oxide)–poly(ethylene oxide) (EO–PO–EO) nonionic surfactant (Pluronic P123) as the structure-directing agent [32]. In a typical synthesis procedure, 4.0 g of Pluronic P123 was dissolved in a mixture of 30 g of H_2O and 120 ml of HCl (2 M). To this solution, 8.5 g of tetraethoxysilane (TEOS) was added. The resulting mixture was stirred vigorously for 20 h at 313 K, then heated to 353 K and maintained there for 24 h. The resulting solid was filtered off and washed with deionized water. After drying at 353 K for 24 h, the solid was further dried in vacuo at 353 K for 24 h to yield SBA-15 containing Pluronic P123 (P123@SBA-15).

To modify the external surface of SBA-15 by substituting the outer surface Si–OH groups with Si–CH_3 groups [33], 3.0 g of P123@SBA-15 was dispersed in 100 ml of toluene at 343 K under nitrogen atmosphere, after which 20 ml of $(CH_3)_3SiCl$ was added under stirring. After 24 h of stirring, the mixture was filtered, and the residue was dried in vacuo at 363 K for 12 h. Finally, Pluronic P123 was removed by Soxhlet extraction in refluxing ethanol for 48 h to obtain SBA-CH_3, which was dried in vacuo at 353 K for 24 h and then stored in vacuo.

2.2. Grafting bipyridine groups into SBA–CH_3 and SiO_2

The synthesis of 4,4′-bis(chlorocarbonyl)-2,2′-bipyridine (**1**) was done from commercially available 4,4′-dimethyl-2,2′-bipyridine (dMBpy, Aldrich) as described previously [30,31]. A solution of compound **1** (0.35 g, 1.25 mmol) in $CHCl_3$ (30 ml) was slowly added dropwise to a stirred mixture solution of 3-aminopropyltriethyloxysilane (APTES, **2**) (0.60 ml, 2.50 mmol, 2 equiv) and triethylamine (0.54 ml, 3.75 mmol, 3 equiv) in $CHCl_3$ (20 ml) for 1 h. The resulting mixture was refluxed under nitrogen atmosphere for 1 h to obtain a 4,4′-bis(chlorocarbonyl)-2,2′-bipyridine bis-[(3-triethyloxysilylpropyl)amide] (**3**) solution. Then 0.5 g of SBA-CH_3 was suspended into this solution, and the mixture thus obtained was stirred overnight at room temperature under nitrogen atmosphere. Then the solution was filtered off, and the solid was washed 3 times with $CHCl_3$, H_2O, methanol, and diethyl ether. The solid thus obtained was then dried at 323 K overnight and finally dried in vacuo at room temperature overnight to produce the powder, designated bpy–SBA.

In a procedure similar to described that above for bpy–SBA, the bipyridine groups also were grafted to SiO_2 (Aerosil 300) and dried at 353 K for 24 h before the graft reaction. The bpy–SiO_2 was recovered, washed, and dried under the same conditions as for bpy–SBA.

2.3. Preparation of bpy–SiO_2-CH_3

To substitute the residual Si–OH groups on bpy–SiO_2 with the Si–CH_3 groups, 3.0 g of bpy–SiO_2 was dispersed in 100 ml of toluene at 343 K under nitrogen atmosphere. Then 20 ml of $(CH_3)_3SiCl$ was added to the suspension under stirring. The mixture was then stirred for another 24 h and then filtered, and the resultant solid was dried in vacuo at 363 K for 12 h to obtain bpy–SiO_2–CH_3.

2.4. Preparation of Fe–bpy–SBA(A), Fe–bpy–SiO_2(A), and Fe–bpy–SiO_2–CH_3(A)

In this work, 0.3 g of bpy–SBA, bpy–SiO_2, and bpy–SiO_2–CH_3 were each suspended in 7.5 ml of methanol containing 0.36 mmol of $Fe(ClO_4)_3{\cdot}9H_2O$. After stirring for 0.5 h, 0.72 mmol of bipyridine was added to the mixtures. Then 50.6 μl of Et_3N also was added to the mixtures after stirring for another 3 h. The suspensions were stirred for another 2 h and left overnight at 255 K. The solids were recovered by filtration and washed with methanol and acetone to remove the unreacted reagents until the filtered solvents were clear. The obtained solids were dried at 323 K overnight to yield the powders, designated Fe–bpy–SBA(A), Fe–bpy–SiO_2(A), and Fe–bpy–SiO_2–CH_3(A).

2.5. Preparation of Fe–bpy–SBA(B) and Fe–bpy–SiO_2(B)

In this step, 3 g of either bpy–SBA or bpy–SiO_2 was suspended in 0.36 mmol of $Fe(ClO_4)_3{\cdot}9H_2O$ in 7.5 ml of methanol. After stirring for 3 h, 50.6 μl of Et_3N was added. The suspensions were stirred for another 2 h and left at 255 K overnight. The solids were recovered by the same procedure as used for Fe–bpy–SBA(A) and Fe–bpy–SiO_2(A), with the resulting solids designated Fe–bpy–SBA(B) and Fe–bpy–SiO_2(B).

2.6. Synthesis of Fe_2O complexes/SBA-15

$Fe_2O(bpy)_4(H_2O)_2(ClO_4)_4$ (hereinafter referred to as Fe_2O complex) was synthesized according to procedures reported previously [34]. First, 2 mmol of bipyridine was added to 1 mmol of $Fe(ClO_4)_3{\cdot}9H_2O$ in 20 ml of methanol. The solution turned deep green after the addition of 140 μl of Et_3N. The solution was then left at 255 K to yield a green powder. Fe_2O complex/SBA-15 was prepared by impregnating 0.1 g of SBA–CH_3 in 10 ml of methanol involving 0.1 mmol of $Fe_2O(bpy)_4(H_2O)_2(ClO_4)_4$. The methanol solvent was then further removed by evacuation at room temperature.

2.7. Catalytic activity

First, 30 mg of either Fe–bpy–SBA or Fe–bpy–SiO_2 powder was suspended in 5 ml of CH_3CN containing 3.83 mmol of cyclohexane. The reaction was started by adding 0.5 mmol of *tert*-butyl hydroperoxide (TBHP). After reaction at room temperature for 4 h, 50 μmol of acetophenone was added to the reaction mixtures as an internal standard to monitor the reaction, and the products were analyzed by gas chromatography (Shimadzu GC-2014).

2.8. Catalyst characterization

Elemental analysis of the C and N present in the samples was carried out with an element analyzer (Elementar Vario EL-III) to evaluate the loadings of bipyridine derivatives. The loadings of Fe ions in the obtained samples were determined by atomic absorption flame emission spectrophotometry (AAS, Shimadzu AA-6400F). The UV–vis spectra were recorded with a double-beam digital spectrophotometer (Shimadu UV-2200A) using $BaSO_4$ powder as a reference. The FT-IR spectra were recorded with an FT-IR spectrometer (JASCO FT-IR 7300) using a TGS detector under a nominal resolution of 2 cm^{-1}, with 100 scans obtained in the transmission mode averaged. The ESR spectra were recorded with a JES-RE2X spectrometer operating in the X-band mode. The XAFS spectra at the Fe K-edge were measured at the BL-12C station in the Photon Factory at the High-Energy Accelerator Research Organization (KEK-PF, Tsukuba), with the samples evaluated in the

Table 1
Results of H, C, N analyses and the loadings of the bipyridine units and Fe^{3+} ions

Samples	Fe (wt%)	Element analysis (mmol/g)			bpy[a] (mmol/g)
		C	H	N	
bpy–SBA	0	13.00	32.70	1.04	0.26
Fe–bpy–SBA(A)	1.34	11.08	30.30	1.00	n.d.[b]
Fe–bpy–SBA(B)	2.60	9.53	29.00	0.91	0.23
bpy–SiO_2	0	4.03	10.20	0.84	0.21
Fe–bpy–SiO_2(A)	2.14	4.93	15.00	0.99	n.d.
Fe–bpy–SiO_2(B)	2.94	3.50	13.10	0.74	0.19
bpy–SiO_2–CH_3	0	5.21	13.30	0.84	0.21
Fe–bpy–SiO_2–CH_3(A)	1.62	5.18	14.00	0.76	n.d.

[a] Bipyridine units grafted onto the surface of the channels of SBA-15 were calculated on the basis of the N content.
[b] n.d.—undetermined.

fluorescence mode at room temperature. X-rays from the storage ring (2.5 GeV) were monochromatized with a Si(111) double-crystal monochromator. EXAFS analysis was carried out using the REX2000 programs for background removal and nonlinear least squares fitting of the data.

3. Results and discussion

Our previous research suggested that bipyridine units are covalently anchored onto the surface of SiO_2 or SBA-15 by a reaction of the silane groups of the bipyridine derivatives with the Si–OH groups present in SiO_2 and SBA-15. Elemental analysis demonstrated 0.21–0.26 mmol of bipyridine units anchored on the surface of 1 g of bpy–SBA and bpy–SiO_2 (Table 1). The reaction of bpy–SiO_2 with $(CH_3)_3SiCl$ led to almost no change in the N content, whereas a higher C content was present in bpy–SiO_2–CH_3 than bpy–SiO_2. These results indicate that at least some parts of the residual Si–OH groups present in bpy–SiO_2 were further substituted by the Si–CH_3 groups. Although Fe–bpy–SBA(A) and Fe–bpy–SiO_2(A) exhibited lower loadings of Fe ions, their C and N contents were higher than for those of Fe–bpy–SBA(B) and Fe–bpy–SiO_2(B), respectively. The bipyridine molecules in solution, together with the anchored bipyridine units, may have reacted with the Fe^{3+} ions as ligands to form Fe bipyridine complexes in Fe–bpy–SBA(A) and Fe–bpy–SiO_2(A); however, only the anchored bipyridine units reacted with the Fe^{3+} ions for the formation of Fe bipyridine complexes in Fe–bpy–SBA(B) and Fe–bpy–SiO_2(B).

The reaction of the bipyridine units anchored inside SBA-15 with the Fe^{3+} ions led to new UV–vis absorption bands in the range of 300–600 nm compared with bpy–SBA, as shown in Fig. 1. The Fe bipyridine complexes formed inside the mesopores of SBA-15 or on the surface of SiO_2 showed similar UV–vis spectra as those for the Fe_2O complexes impregnated in SBA-15, in good agreement with the Fe_2O complexes reported previously [34,35]. The absorption bands at 300–400 nm were assigned to the $O^{2-} \rightarrow Fe^{3+}$ charge-transfer transition [35]. On the other hand, the absorption bands between 400 and 600 nm were similar in position and intensity to the $^6A_1 \rightarrow {}^4T_2({}^4G)$ and $^6A_1 \rightarrow ({}^4A_1, {}^4E)({}^4G)$ transitions observed in other high-spin, octahedral Fe^{3+} complexes [36]. The UV–vis absorption spectra of Fe–bpy–SiO_2(A) and Fe–bpy–SBA(A) shifted toward shorter wavelengths compared with those of Fe–bpy–SiO_2(B) and Fe–bpy–SBA(B), respectively. Based on these findings, it can be concluded that the polarity of the surroundings of the Fe^{3+} ions increased as these ions interacted with more bipyridine molecules present in Fe–bpy–SiO_2(A) and Fe–bpy–SBA(A), according to the Lippert equation [37]. Moreover, the Fe^{3+} bipyridine complexes anchored inside SBA-15 (Fe–bpy–SBA), as well as the Fe_2O complex impregnated in SBA-15, demonstrated UV–vis absorption at shorter wavelengths compared with those anchored on SiO_2 (Fe–bpy–SiO_2). These findings suggest that the Fe^{3+} bipyridine complexes present in SBA-15 are of higher polarity

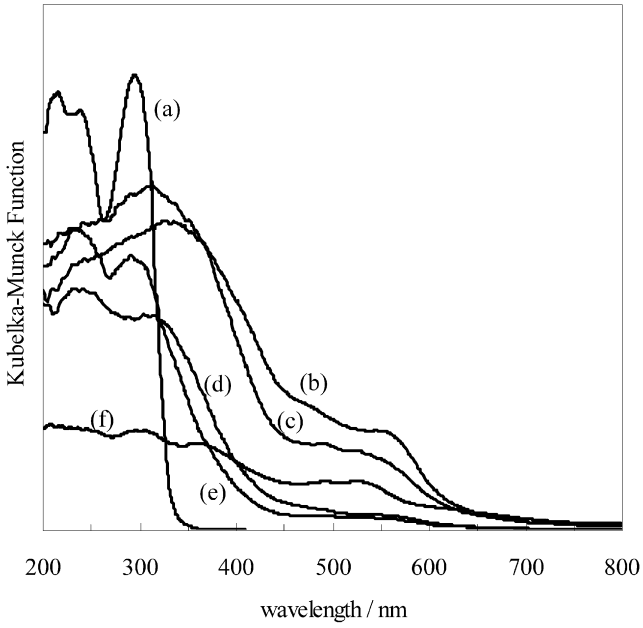

Fig. 1. UV–vis spectra of: (a) bpy–SBA, (b) Fe–bpy–SiO_2(B), (c) Fe–bpy–SiO_2(A), (d) Fe–bpy–SBA(B), (e) Fe–bpy–SBA(A) and (f) Fe_2O complexes/SBA-15.

than those present on the surface of SiO_2. Such high polarity may be closely associated with the constrained structure of the complexes within the nanopores of SBA-15 [38].

As shown in Fig. 2, bpy–SiO_2 and bpy–SBA exhibited resolved absorptions at 1550 cm^{-1} due to the bending vibrations of N–H [39], along with broad FT-IR bands at 1650–1570 cm^{-1}. The bands at 1638 cm^{-1} can be assigned to the stretching vibrations of CONH, and the absorption bands at 1598 cm^{-1} as well as the broad absorption at 1475–1463 cm^{-1} are characteristic of anchored bipyridine derivatives [39]. The results of FT-IR measurements show that the bipyridine derivatives were anchored successfully on the surface of bpy–SiO_2 or on the inner surface of the mesopores of bpy–SBA. In contrast, both Fe–bpy–SiO_2(A) and Fe–bpy–SBA(A) exhibited highly resolved absorption bands at 1605, 1475, and 1445 cm^{-1} that were not seen in Fe–bpy–SiO_2(B) and Fe–bpy–SBA(B). These bands were also observed on the Fe_2O complexes impregnated in SBA-15, however. These absorptions are attributed to the 2,2′-bipyridine complexed with Fe^{3+} ions, which were observed at slightly higher frequencies compared with uncomplexed 2,2′-bipyridine [40]. It was confirmed that not only the anchored bipyridine units, but also the free bipyridine molecules, reacted with the Fe^{3+} ions together as ligands to form Fe bipyridine complexes in Fe–bpy–SBA(A) and Fe–bpy–SiO_2(A). Moreover, the absorption bands at 772 cm^{-1}, attributed to the asymmetric Fe–O–Fe stretching vibration [36], were clearly seen in the Fe–bpy–SBA(A) and Fe_2O complexes impregnated in SBA-15. The μ–oxo diferric complexes were found to be formed successively inside the mesopores of Fe–bpy–SBA(A), whereas no formation of a Fe–O–Fe structure in Fe–bpy–SBA(B) occurred, due to absence of the absorption bands at 772 cm^{-1}. But distinguishing the absorption bands at 772 cm^{-1} for Fe–bpy–SiO_2(A) and Fe–bpy–SiO_2(B) is difficult, because the FT-IR spectra are very broad in these areas.

Except for Fe–bpy–SBA(B), all of the samples measured at 298 K showed similar ESR spectra, as shown in Fig. 3, with sharp signals at $g = 4.1$ and broad signals at $g = 2.0$ characteristic of a high-spin character and non-heme ferric system with rhombic symmetry [41]. The signals at $g = 4.1$ can be assigned to the magnetically noninteracting Fe^{3+} species, which is an impurity normally appearing in binuclear ferric complexes [41]. In contrast, the signals at

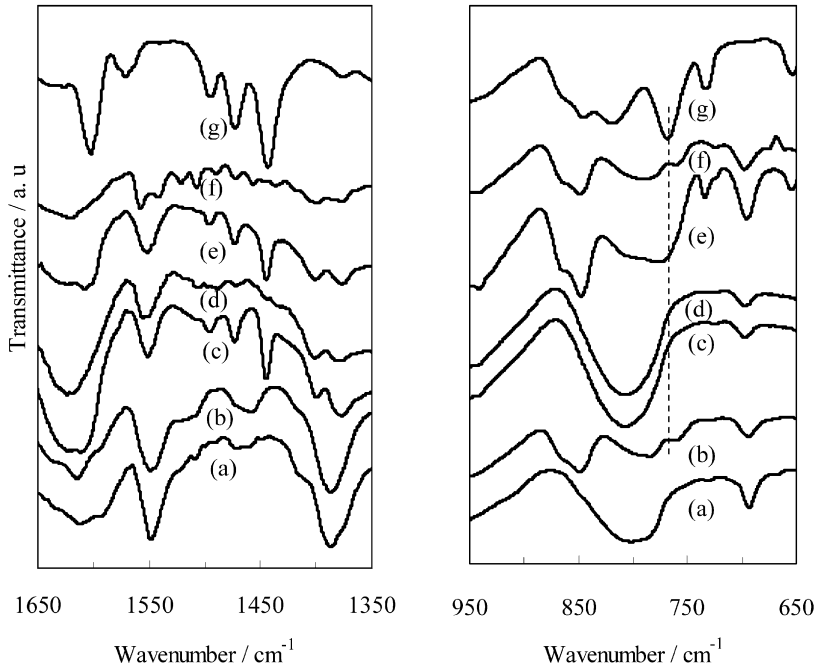

Fig. 2. FT-IR spectra of: (a) bpy–SiO_2, (b) bpy–SBA, (c) Fe–bpy–SiO_2(A), (d) Fe–bpy–SiO_2(B), (e) Fe–bpy–SBA(A), (f) Fe–bpy–SBA(B), and (g) Fe_2O complexes/SBA-15.

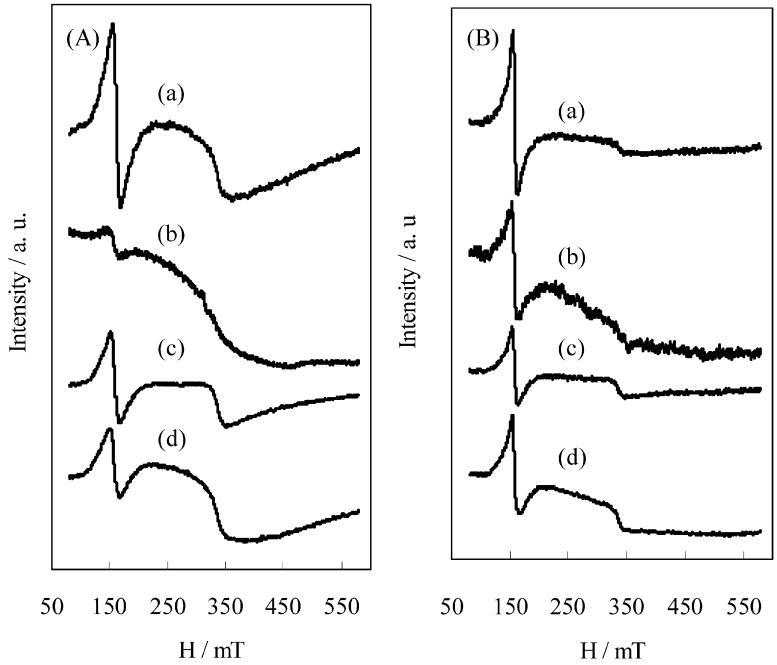

Fig. 3. ESR spectra of: (a) Fe–bpy–SBA(A), (b) Fe–bpy–SBA(B), (c) Fe–bpy–SiO_2(A), and (d) Fe–bpy–SiO_2(B) measured at (A) 298 K and (B) 77 K.

$g = 2.0$ correspond to the antiferromagnetically coupled binuclear iron species [42], the ESR signals of which were almost silent at 77 K, in obvious deviation from Curie's law. As shown in Fig. 3, formation of the Fe–O–Fe binuclear iron species in Fe–bpy–SBA(A) was evidenced by ESR measurements in good agreement with the FT-IR measurements. Although a decreased intensity of the ESR signals at $g = 2.0$ also was seen at 77 K for both the Fe–bpy–SiO_2(A) and Fe–bpy–SiO_2(B) catalysts, fairly strong signals at $g = 2.0$ could still be observed, and these were assigned to the presence of the aggregated Fe^{3+} species of these catalysts [43]. These results indicate that some Fe–O–Fe binuclear iron species may have been anchored onto Fe–bpy–SiO_2 together with some aggregated Fe^{3+} species possibly formed from the reaction of $Fe(ClO_4)_3$ with the Si–OH groups present on the surface of SiO_2.

All of the samples exhibited almost the same Fe K-edge XANES spectra with the pre-edge peaks at 7113.5 eV due to the 1s → 3d transitions of the Fe^{3+} ions [44], as shown in Fig. 4A. Nevertheless, obvious differences can be seen in the FT-EXAFS spectra of the Fe bipyridine complexes anchored on SiO_2 and SBA-15, which exhibit characteristic peak patterns of metalloporphyrin, as reported previously [45–47]. The crystalline samples ($Fe(bpy)_3(ClO_4)_3 \cdot 3H_2O$, α-Fe_2O_3) were used as reference compounds, and the EXAFS backscattering amplitude and phase factors were extracted using the distances of Fe–N and Fe–Fe from the XRD data for the refer-

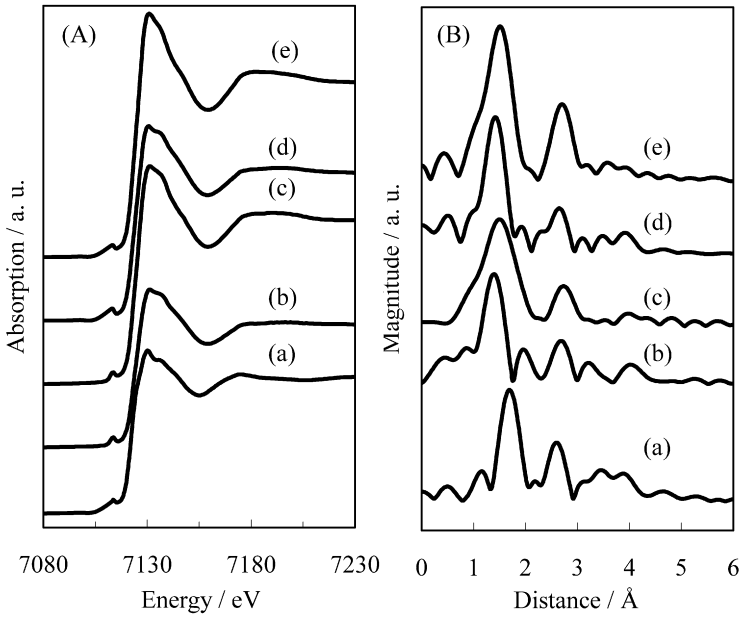

Fig. 4. XANES (A) and FT-EXAFS (B) spectra of: (a) Fe_2O complexes, (b) Fe–bpy–SBA(A), (c) Fe–bpy–SBA(B), (d) Fe–bpy–SiO_2(A), and (e) Fe–bpy–SiO_2(B).

Table 2
Results of the curve-fitting of the Fourier-filtered $k^3\chi(k)$ Fe K-edge EXAFS of Fe–bpy–SiO_2 and Fe–bpy–SBA[a]

Samples	Shell	R (Å)	CN	σ^2 (Å^2)	ΔE_0 (eV)	F
Fe–bpy–SBA(A)	Fe–N(O)	1.78	6.00	0.024	−9.6	0.26
	Fe-Fe	3.53	0.74	0.040	−7.3	0.43
Fe–bpy–SBA(B)	Fe–N(O)	1.83	3.99	0.079	−10.7	0.51
Fe–bpy–SiO_2(A)	Fe–N(O)	1.88	5.84	0.072	−12.0	0.47
	Fe–Fe	3.48	1.07	0.079	−8.7	0.53
Fe–bpy–SiO_2(B)	Fe–N(O)	1.89	4.09	0.087	−7.2	0.35
Fe_2O complex	Fe–N(O)	2.08	5.96	0.014	−10.6	0.21
	Fe–Fe	3.57	0.95	0.065	−8.7	0.49
$Fe(bpy)_3(ClO_4)_3{\cdot}3H_2O$	Fe–N	1.97	6			
α–Fe_2O_3	Fe–Fe	2.95	4			

[a] Fourier transformed range: $k = 2.0$–14.0 Å^{-1}; R: bond distance; CN: coordination number; σ^2: Debye–Waller factor; ΔE_0: threshold energy; F: fit quality defined as $[\sum(\chi_o - \chi_c)^2 k^6 / \sum \chi_o^2 k^6]$ (χ_o = observed EXAFS; χ_c = calculated EXAFS); errors are estimated to be 25% for coordination numbers and ±0.05 Å for distances.

ence compounds [47–49]. The curve-fitting results for the Fourier-filtered $k^3\chi(k)$ Fe K-edge EXAFS are given in Table 2. The strong first peaks shown in Fig. 4B at 1.5–2.0 Å, before phase-shift correction, represent the Fe–O_{bridge}, Fe–O_{water}, and Fe–N_{ligand} distances. It was difficult to resolve the Fe–O_{bridge} distance from the Fe–O_{water} and Fe–N_{ligand} distances, due to the negligible difference in these distances. The neighboring atomic numbers of O and N, as well as the distances of Fe–O and Fe–N, were treated as a single nitrogen shell in the analysis. EXAFS curve-fitting analysis revealed that the average Fe-first shell atom distances of Fe–bpy–SBA and Fe–bpy–SiO_2 were shorter than those in the Fe_2O complex. Similar EXAFS findings were reported by Wasielewski et al. [47], demonstrating that the peak can be ascribed to the Fe^{3+} ions binding to the bipyridine units with a bidentate configuration different from that of the Fe_2O complex. The second peak and shoulder combination at 2.4–3.0 Å, before phase-shift correction, were assigned to the backscattering from the carbon atoms adjacent to the ligating N atoms of the bipyridine ring [48]. Furthermore, both the Fe_2O complexes and Fe–bpy–SBA(A) exhibited peaks at around 3.2 Å before phase-shift correction, as shown in Fig. 4B. Taking into account that the phase-shift correction was approximately 0.3 Å and the distance of Fe–Fe was crystallographically determined to be 3.535 Å for the Fe_2O complexes [36], the peak at 3.2 Å can be assigned to backscattering from the neighboring Fe atoms. Despite the Fe^{3+} bipyridine complexes formed inside SBA-15 with a different configuration from the Fe_2O complex, the backscattering from the neighboring Fe atoms observed in Fe–bpy–SBA(A) confirms the presence of a similar structure for Fe–O–Fe in Fe–bpy–SBA(A) as in the Fe_2O complex. The presence of the Fe–O–Fe structure in Fe–bpy–SBA(A) demonstrated by XAFS measurements also indicates good agreement with the FT-IR and ESR measurements. But no peaks at around 3.2 Å were observed on Fe–bpy–SBA(B), indicating absence of the Fe–O–Fe structure for the Fe^{3+} bipyridine complexes present in Fe–bpy–SBA(B). The backscattering from the neighboring Fe atoms was observed for Fe–bpy–SiO_2(A) at a slightly shorter distance than for Fe–bpy–SBA(A), suggesting that the angle of the Fe–O–Fe linkage present in Fe–bpy–SiO_2(A) may be larger than that present in Fe–bpy–SBA(A), due to confinement of the di-iron complexes formed inside the mesoporous channels.

Table 3
Yields of cyclohexanol (cyOH) and cyclohexanone (cyONE) in the oxidation of cyclohexane by TBHP[a]

Catalysts	TBHP conversion (%)	Products (μmol)		Yields[b] (%)	cyOH/cyONE ratio
		cyOH	cyONE		
Fe_2O complex[c]	99.9	51.6	60.1	31.7	0.9
Fe–bpy–SBA(A)	95.7	46.5	90.0	43.7	0.5
Fe–bpy–SBA(B)	33.0	8.9	1.9	7.1	6.1
Fe–bpy–SiO_2(A)	98.5	42.8	80.7	38.3	0.5
Fe–bpy–SiO_2(B)	53.3	22.2	22.8	23.4	1.0
Fe–bpy–SiO_2–CH_3(A)	52.5	29.3	26.5	28.9	1.0

[a] Reaction conditions: room temperature in CH_3CN; reaction time: 4 h.
[b] Total yield based on oxidant. The ketone yields are the molar yields multiplied by 2 since 2 equiv of TBHP are required to produce one equiv of ketone.
[c] 3.5 μmol; with catalyst: TBHP = 1:143 (molar ratio); the turnover numbers of cyOH and cyONE for the Fe_2O complex were 14.8 and 17.2, respectively.

Table 3 compares the catalytic activity of the anchored di-iron complexes on SiO_2 and inside SBA-15 for the oxidation of cyclohexane with TBHP. Fe–bpy–SBA(A) exhibited much greater activity than Fe–bpy–SBA(B), which can be attributed to the presence of the μ–oxo-bridged binuclear Fe complex species, which have been suggested to be the active species for the oxidation of cyclohexane [34,36]. More Fe complexes were present in Fe–bpy–SiO_2(A), which demonstrated almost the same activity as Fe–bpy–SBA(A). Thus, the Fe complexes present in Fe–bpy–SBA(A) exhibited greater ac-

tivity than those present in Fe–bpy–SiO_2(A). This can be attributed to the formation of more binuclear Fe complexes inside SBA-15 or to the effect of the mesopore channels of SBA-15, which can act as a nanoreactor concentrating the substrates in proximity to the binuclear Fe complexes [15]. In addition, both Fe–bpy–SBA(A) and Fe–bpy–SiO_2(A) exhibited much higher selectivity for the oxidation of cyclohexane into cyclohexanone compared with the unsupported Fe_2O complexes.

For the oxidation of cyclohexane with TBHP that occurred on the binuclear Fe complexes, binuclear Fe complexes have been suggested to act as catalysts for the hemolytic decomposition of TBHP ($2^tBuOOH \rightarrow {}^tBuO\cdot + {}^tBuOO\cdot + H_2O$) over other pathways. The produced radicals from TBHP then induce the successive oxidation of cyclohexane [50]. Cyclohexyl hydroperoxide (cyOOH) is believed to be an intermediate for the production of cyclohexanol (cyOH) and cyclohexanone (cyONE) [51]. It was found that the removal of the Si–OH groups present in Fe–bpy–SiO_2(A) led to much lower activity for Fe–bpy–SiO_2–CH_3(A). Nevertheless, Fe–bpy–SiO_2–CH_3(A) showed similar selectivity for the oxidation of cyclohexane into cyclohexanone as the unsupported Fe_2O complexes. Fish et al. [52] investigated the effect of a solvent on the homogeneous cyclohexane oxidation over Fe_2O complexes with TBHP and found that the aqueous reaction solution of pH 4.2 gave cyclohexanone as the predominant product. The surface –OH groups were present on the surface of SiO_2/SBA-15 and may have coordinated with the Fe^{3+} ion center instead of water to form Fe^{3+} bipyridine complexes with the (Si–O(H)–Fe) structure, in which Brönsted acid sites were formed. These Brönsted acid sites may have interacted with cyOOH, contributing to the high selectivity for the formation of cyclohexanone with the supported μ–oxo-bridged binuclear Fe complex catalysts prepared on SBA-15 or SiO_2.

4. Conclusion

Fe^{3+} bipyridine complexes were successfully synthesized and anchored on the surface of SiO_2 or inside the mesopores of SBA-15. FT-IR, ESR, and XAFS measurements confirmed the formation of an μ–oxo–bridged binuclear Fe species in Fe–bpy–SiO_2(A) and Fe–bpy–SBA(A), which were the active species for the oxidation of cyclohexane. Furthermore, the binuclear Fe complexes anchored inside the mesopores of SBA-15 [Fe–bpy–SBA(A)] exhibited much greater activity than those anchored on the surface of SiO_2. The supported binuclear Fe complexes exhibited higher selectivity for the oxidation of cyclohexane into cyclohexanone than the unsupported binuclear Fe complexes, due to the presence of Si–OH groups on the surface of SiO_2 or inside the mesopores of SBA-15.

References

[1] B.R. Wood, J.A. Reimer, A.T. Bell, M.T. Janicke, K.C. Ott, J. Catal. 225 (2004) 300.
[2] S.R. Blaszkowski, R.A. Van Santen, J. Am. Chem. Soc. 118 (1996) 5152.
[3] G. Zhu, K. Fujimoto, D.Y. Zemlyanov, A.K. Datye, F.H. Ribeiro, J. Catal. 225 (2004) 170.
[4] H. Dalton, Adv. Appl. Microbiol. 26 (1980) 71.
[5] M.H. Baik, M. Newcomb, R.A. Friesner, S.J. Lippard, Chem. Rev. 103 (2003) 2385.
[6] B.J. Wallar, J.D. Lipscomb, Chem. Rev. 96 (1996) 2625.
[7] M. Costas, K. Chen, L. Que, Coord. Chem. Rev. 200 (2000) 517.
[8] M. Fontecave, S. Menage, C. Duboc-Toia, Coord. Chem. Rev. 180 (1998) 1555.
[9] M. Kodera, M. Itoh, K. Kano, T. Funabiki, M. Reglier, Angew. Chem. Int. Ed. 44 (2005) 7104.
[10] C. Marchi-Delapierre, A. Jorge-Robin, A. Thibon, S. Menage, Chem. Commun. (2007) 1166.
[11] M. Yamakawa, H. Ito, R. Noyori, J. Am. Chem. Soc. 122 (2000) 1466.
[12] F. Simal, L. Wlodarcazk, A. Demonceau, A.F. Noels, Eur. J. Org. Chem. (2001) 2689.
[13] J.M. Thomas, R. Raja, D.W. Lewis, Angew. Chem. 117 (2005) 6614.
[14] M. Tada, R. Coquet, J. Yoshida, M. Kinoshita, Y. Iwasawa, Angew. Chem. Int. Ed. 46 (2007) 7220.
[15] K. Feng, R.Y. Zhang, L.Z. Wu, B. Tu, M.L. Peng, L.P. Zhang, D. Zhao, C.H. Tung, J. Am. Chem. Soc. 128 (2006) 14685.
[16] J.V. Nguyen, C.W. Jones, Macromolecules 37 (2004) 1190.
[17] R. Ganesan, B. Viswanathan, J. Mol. Catal. A 181 (2002) 99.
[18] K.F. Mongey, J.G. Vos, B.D. MacCraith, C.M. McDonagh, C. Coates, J.J. McGarvey, J. Mater. Chem. 7 (1997) 1473.
[19] M. Ogawa, T. Nakamura, J.I. Mori, K. Kuroda, Microporous Mesoporous Mater. 48 (2000) 159.
[20] M.M. Collinson, B. Novak, M. Skylar, J.S. Taussig, Anal. Chem. 72 (2000) 2914.
[21] P.K. Gosh, T.G. Spiro, J. Am. Chem. Soc. 102 (1980) 5543.
[22] K.A. Cheng, W.Y. Lin, S.G. Li, C.M. Che, W.Q. Pang, New J. Chem. 23 (1999) 733.
[23] H.R. Li, J. Lin, H.J. Zhang, H.C. Li, L.S. Fu, Q.G. Meng, Chem. Commun. (2001) 1212.
[24] F. Odobel, B. Bujoli, D. Massiot, Chem. Mater. 13 (2001) 163.
[25] F. Odobel, D. Massiot, B.S. Harrison, K.S. Schanze, Langmuir 19 (2003) 30.
[26] Y. Sato, M. Kagotani, Y. Souma, J. Mol. Catal. A 151 (2000) 79.
[27] Y. Shen, S. Zhu, Macromolecules 34 (2001) 8603.
[28] M.T. Bore, H.N. Pham, E.E. Switzer, T.L. Ward, A. Fukuoka, A.K. Datye, J. Phys. Chem. B 109 (2005) 2873.
[29] M.T. Bore, H.N. Pham, T.L. Ward, A.K. Datye, Chem. Commun. 22 (2004) 2620.
[30] N. Garelli, P. Vierling, J. Org. Chem. 57 (1992) 3046.
[31] L.H. Uppadine, F.R. Keene, P.D. Beer, J. Chem. Soc. Dalton Trans. (2001) 2188.
[32] D. Zhao, Q. Hou, J. Feng, B.F. Chmelka, G.D. Stuky, J. Am. Chem. Soc. 120 (1998) 6024.
[33] L. Li, J.L. Shi, L.Z. Zhang, L.M. Xiong, J.N. Yan, Adv. Mater. 16 (2004) 1079.
[34] S. Menage, J.M. Vincent, C. Lambeaux, G. Chottard, A. Grand, M. Fontecave, Inorg. Chem. 32 (1993) 4766.
[35] J.E. Plowman, T.M. Loehr, C.K. Schauer, O.P. Anderson, Inorg. Chem. 23 (1984) 3553.
[36] D.M. Kurtz, Chem. Rev. 90 (1990) 585.
[37] R. Lakowicz, Principles of Fluorescence Spectroscopy, Plenum Press, New York, 1983, p. 190.
[38] Q.H. Xu, L.S. Li, X.S. Liu, R.R. Xu, Chem. Mater. 14 (2002) 549.
[39] H.R. Li, J. Lin, H.J. Zhang, H.C. Li, L.S. Fu, Q.G. Meng, Chem. Commun. (2001) 1212.
[40] J. Morizzi, M. Hobday, C. Rix, Inorg. Chim. Acta 320 (2001) 67.
[41] C.L. Liu, S.W. Yu, D.F. Li, Z.R. Liao, X.H. Sun, H.B. Xu, Inorg. Chem. 41 (2002) 913.
[42] R. Ganesan, B. Viswanathan, J. Mol. Catal. A 181 (2002) 99.
[43] D. Skrzypek, B. Szymanska, D. Kovala-Demertzi, J. Wiecek, E. Talik, M.A. Demertzis, J. Phys. Chem. Solids 67 (2006) 2550.
[44] L.X. Chen, Z. Wang, J.K. Burdett, P.A. Montano, J.R. Norris, J. Phys. Chem. 99 (1995) 7958.
[45] S. Kim, D.A. Tryk, I.T. Bae, M. Sandifer, R. Carr, M.R. Antonio, D.A. Scherson, J. Phys. Chem. 99 (1995) 10359.
[46] J.U. Rohde, S. Torelli, X. Shan, M.L. Lim, E.J. Klinker, J. Kaizer, K. Chen, W. Nam, L. Que, J. Am. Chem. Soc. 126 (2004) 16750.
[47] L.X. Chen, W.J.H. Jager, D.J. Gosztola, M.P. Niemczyk, M.R. Wasielewski, J. Phys. Chem. B 104 (2000) 1950.
[48] L.M.L. Daku, A. Vargas, A. Hauser, A. Fouqueau, M.E. Casida, ChemPhysChem 6 (2005) 1393.
[49] A.A. Battiston, J.H. Bitter, F.M.F. de Groot, A.R. Overweg, O. Stephan, J.A. van Bokhoven, P.J. Kooyman, C. van der Spek, G. Vanko, D.C. Koningsberger, J. Catal. 213 (2003) 251.
[50] Z. Hu, S.M. Gorun, B. Meunier (Eds.), Biomimetic Oxidations Catalyzed by Transition Metal Complexes, Imperial College Press, London, 2000, p. 293.
[51] R.H. Fish, M.S. Konings, K.J. Oberhausen, R.H. Fong, W.M. Yu, G. Christou, J.B. Vincent, D.K. Coggin, R.M. Buchanan, Inorg. Chem. 30 (1991) 3002.
[52] A. Rabion, S. Chen, J. Wang, R.M. Buchanan, J.L. Seris, R.H. Fish, J. Am. Chem. Soc. 117 (1995) 12356.